Meccanica (2013) 48:567–583
DOI 10.1007/s11012-012-9616-4

Centreline velocity decay characterisation in low-velocity jets downstream from an extended conical diffuser

X. Grandchamp · A. Van Hirtum · X. Pelorson

Received: 16 September 2011 / Accepted: 17 September 2012 / Published online: 5 October 2012

Abstract The centreline velocity decay of round airflow jets issuing from extended conical diffusers with length-to-diameter ratio $1.2 \leq L_t/d \leq 20$ is studied for moderate bulk Reynolds numbers $1131 \leq Re_b \leq 9054$. The centreline velocity decay varies as a function of the initial conditions. The functional correlation between the centreline velocity decay coefficient and the initial centreline turbulence level observed on convergent nozzles (Malmström et al. in J. Fluid Mech. 246:363–377, 1997) breaks down as the initial centreline turbulence level exceeds 20 %. In addition, the centreline velocity decay coefficient expressed as function of the bulk velocity U_b decreases for $U_b <$ 3 m/s instead of initial mean velocity $U_0 < 6$ m/s as reported for convergent nozzles (Malmström et al. in J. Fluid Mech. 246:363–377, 1997). The asymptotic values of the decay coefficient for $U_b > 3$ m/s decrease linearly when expressed as function of the initial centreline turbulence intensity u_0/U_0. Studied flow and geometrical conditions are relevant to flow through the human upper airways.

Keywords Axisymmetrical jet · Moderate Reynolds number jet · Initial conditions · Centreline decay · Upper airway flow

X. Grandchamp · A. Van Hirtum (✉) · X. Pelorson
GIPSA-lab, UMR CNRS 5216, Grenoble University, Grenoble, France
e-mail: annemie.vanhirtum@gipsa-lab.grenoble-inp.fr

List of symbols

ν	kinematic viscosity of air 1.5×10^{-5} m^2/s
d	exit diameter of the nozzle [m]
L_t	length of uniform circular tube extension [m]
d_{in}	minimum diameter of conical diffuser [m]
L_{diff}	length of diverging portion of conical diffuser [m]
L_N	nozzle length $L_N = L_{diff} + L_t$ [m]
x	longitudinal distance from nozzle exit $x = 0$ [m]
y	transverse distance from nozzle centreline $y = 0$ [m]
Δx	longitudinal spatial measurement step [m]
Δy	transverse spatial measurement step [m]
$d_{x/d}$	local jet width at distance x/d from the nozzle exit $x = 0$ [m]
θ	total jet spreading angle [°]
Q_b	volume airflow rate [m^3/s]
U_b	initial bulk centreline velocity at the nozzle exit $x = 0$ assuming an ideal fluid, $U_b = (4Q_b)/(\pi d^2)$ [m/s]
U_0	initial centreline mean velocity at the nozzle exit $x = 0$ [m/s]
Re_b	bulk Reynolds number $Re_b = U_b d/\nu$ or $Re_b = 4Q_b/\pi d\nu$
Re_0	initial Reynolds number $Re_0 = U_0 d/\nu$
$Re_{x/d}$	local Reynolds number $Re_{x/d} = d_{x/d} U_c/\nu$
$Re_{\max}$	maximum local Reynolds number $Re_{\max}(x/d) = \max(Re_{x/d})$
$U_c(x)$	mean bulk centreline velocity [m/s]

$U(y)$	mean transverse velocity at the nozzle outlet $-d/2 \leq y \leq d/2$ at $x/d < 0.04$ [m/s]
$U_{c,p}$	pth instantaneous velocity sample along the centreline [m/s]
N_{tot}	total number of instantaneous velocity samples at a given location
u	velocity root mean square [m/s]
u_0	velocity root mean square at nozzle exit $x = 0$ [m/s]
K	mean centreline velocity decay coefficient
K_1	mean centreline velocity decay coefficient $K_1 = \frac{U_0 K}{U_b}$
K_w	mean transverse velocity decay coefficient $K_w = \frac{\sqrt{0.5 \ln 2}}{\tan\theta/2}$
x_0	virtual origin [m]
x_{pc}	potential core extent [m]
$x_{\max}$	centreline distance corresponding to $Re_{\max}$ [m]

1 Introduction

Due to numerous experimental and numerical studies of round free jet flows, an overall good knowledge and understanding of these flows exist for long pipes and smooth convergent contraction nozzles [5, 7, 15]. The time averaged turbulent jet flow mixing region is schematically divided into three parts: an initial near field region downstream the exit, a transition region and a self-preserving far field region further downstream. Approximate solutions, describing the far field flow evolution, assume the mean streamwise centreline velocity U_c to decrease proportional to $1/x$, where x indicates the streamwise direction from the tube exit. In this third zone, the mean centreline velocity is typically modelled by a simple decay equation [30]:

$$\frac{U_c(x)}{U_0} = K \frac{d}{x - x_0}, \tag{1}$$

where U_c denotes the mean centreline velocity downstream the nozzle exit in the streamwise x direction, d the nozzle exit diameter, U_0 the initial mean centreline velocity at the nozzle exit, K the mean centreline velocity decay coefficient and x_0 the virtual origin. Despite the described universal behaviour it is shown analytically [11, 12] that the mean centreline velocity decay, and so the decay coefficients K and x_0, also depends on Reynolds number as well as on initial conditions at the exit of the emitting geometry such as exit Reynolds number [5, 25, 27], turbulence intensity [6, 24, 28, 32] and upstream nozzle geometry [6, 9, 20–22, 26, 28, 34].

These former investigations are essentially conducted for high bulk Reynolds number flows, typically 10^4 or higher and for geometrical configurations either aiming optimal convergent nozzle design for technological jet applications or developed pipe flow for which the length-to-diameter ratio of the pipe L_t/d exceeds 40. In general, it is observed that for decreasing Reynolds numbers the velocity decays increases [1, 18, 19, 25] and as a result the potential core extent gets shorter [1, 19, 25]. However, the opposite is reported in [18] where for increasing Reynolds number in the range $177 \leq Re_b \leq 5142$ [18], the potential core extent decreases. Consequently, additional streamwise centreline velocity measurements for moderate Reynolds number round jet flow are needed.

In [19] the evolution of the decay constant K and initial mean centreline velocity U_0 for jets issuing from a convergent nozzle at moderate velocities $2 \leq U_0 \leq 12$ m/s is found to be described by a single curve. Moreover, the decay constant is reported to be constant for $U_0 > 6$ m/s. In the current study it is aimed to consider mean centreline velocity behaviour of a moderate Reynolds number jet issuing from a conical diffuser extended with uniform tubes of varying length-to-diameter ratio $L_t/d < 40$. The jet centreline velocity downstream the nozzle is measured for different initial centreline velocities $0.9 < U_0 < 10$ m/s. The influence of varying flow and geometrical configurations on centreline decay rate K, virtual origin x_0 and potential core length x_{pc} are quantified. Next, the decay equation is used to model the streamwise centreline velocity profile and the model performance is evaluated.

The chosen geometrical and flow conditions, i.e. moderate Reynolds numbers and relatively short conical extended diffusers, are e.g. relevant to describe flow through the human vocal tract, for which both the lack and need of flow data in relation to speech production studies is explicitly pointed out [4, 16]. The human upper airways geometry is schematically depicted in Fig. 1 [8, 31]. Variation of the geometrical length scale, corresponding to varying the extension length L_t, is among others due to aging, morphology, pathology or articulation during speech production. During human speech production, a narrowed upstream passage is present at the larynx (glottis), the lips, or naturally created somewhere in the oropharynx during

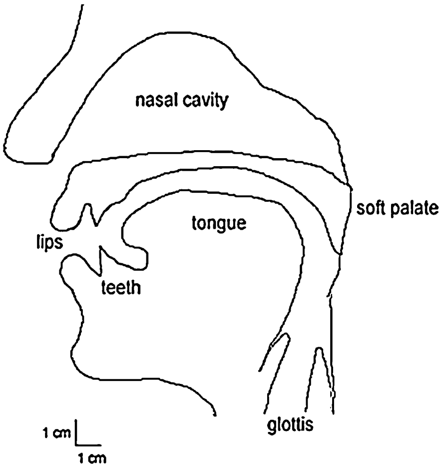

Fig. 1 Sagittal view of human upper airways indicating vocal tract articulators [8, 31]. During human speech production, a constriction might occur at any location along the vocal tract, i.e. from the glottis up to the lips. In the following, the unconstricted vocal tract portion is represented by a uniform circular tube which is connected to a constriction represented by a conical diffuser. The length of the uniform circular tube is varied in order to represent different constriction locations. The resulting extended conical diffuser is schematically depicted in Fig. 2

sound production [8, 31]. The unconstricted vocal tract portion is represented by a uniform circular tube which is connected to a constriction represented by a conical diffuser. The length of the uniform circular tube is varied in order to represent different constrictions locations. Therefore, the vocal tracts geometry is severely simplified as an extended conical diffuser.

2 Extended conical diffuser nozzle

The geometry of the extended conical diffuser nozzle is schematically depicted in Fig. 2. The diffuser nozzle has an inlet diameter of 1 cm, a 14° convergent portion of length 2 cm followed by a 22° divergent portion of length $L_{diff} = 5$ cm. The minimum diameter at the throat of the diffuser yields $d_{in} = 5$ mm and the diffuser outlet diameter d yields 25 mm. The divergent diffuser portion is characterised by an area expansion ratio $d^2/d_{in}^2 = 25$ and a length to inlet diameter ratio $L_{diff}/d_{in} = 10$.

Downstream the diffuser, a uniform circular extension tube of diameter $d = 25$ mm and varying length L_t is added. The assessed extension tube lengths L_t yield 3, 11, 18 and 50 cm. Corresponding length-to-diameter ratios L_t/d yield 1.2, 4.4, 7.2 and 20 based on the exit diameter of the nozzle d. The ratio of the nozzle length, $L_N = L_{diff} + L_t$, downstream from the constriction to the diffusers throat diameter d_{in} yields 120, 280, 420 and 1060, respectively.

Typical quantities observed on the human vocal tract during human speech sound production [8, 31] and quantities characterising the studied diffuser nozzle are given in Table 1. The used extended conical diffuser geometry is in accordance with order of magnitudes associated with the human vocal tract. Therefore, applying volume flow rates Q_b in accordance with observations on human subjects allows to study bulk Reynolds numbers $Re_b < 10^4$ measured on human subjects [8, 31]. Note that an unrealistic extension length of $L_t = 50$ cm is assessed in order to cover the range of L_t/d ratios observed on human subjects.

3 Experimental setup and procedure

The flow facility consists of an air compressor (Atlas Copco GA7) followed by a pressure regulator (Norgren type 11-818-987) providing an airflow at constant pressure. The pressure regulator is connected with a manual valve in order to control the volume flow rate Q_b. The volume flow rate Q_b is measured by a thermal mass flow meter (TSI 4040) with an accuracy of 0.1 l/min. A bulk Reynolds number $Re_b < 10^4$ is imposed during experiments as indicated in Table 1.

The mass flow meter is attached to the extended conical diffuser, schematically depicted in Fig. 2, by a uniform duct of diameter 1 cm and length 50 cm. Downstream from the diffuser, the jet exits in a free field at rest as illustrated by the smoke visualisation in Fig. 3. The rectangular free field chamber has height, width and length corresponding to 120, 120 and 112 times the nozzle outlet diameter d. Except for the air compressor, the complete jet facility is placed inside the closed room for which the temperature is controlled in order to minimise flow disturbances.

A constant temperature anemometer system (IFA 300) is used in order to perform flow velocity measurements. The hot-film is calibrated against the flow meter following the procedure outlined in [14]. Velocity profiles are obtained by moving a single sensor hot film (TSI 1201-20; diameter of 50.8 μm and a working length of 1.02 mm) using a two-dimensional stage positioning system (Chuo precision industrial co. CAT-C, ALS-250-C2P and ALS-115-E1P). The

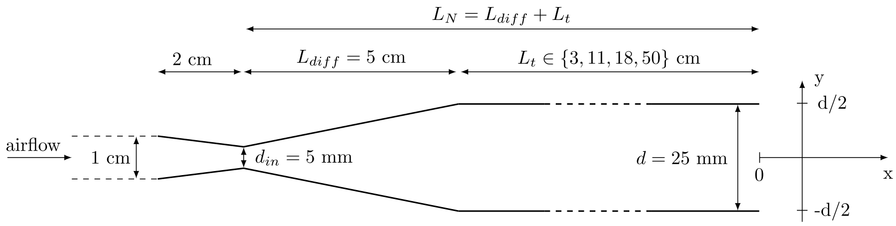

Fig. 2 Extended conical diffuser geometry with variable tube length L_t and constant uniform extension tube diameter d. The longitudinal flow direction x is defined so that $x = 0$ corresponds to the nozzle exit. The origin of the transverse direction y corresponds to the centreline of the nozzle so that the nozzle borders at the exit correspond to $y = -d/2$ and $y = d/2$, respectively

Table 1 Comparison of geometrical and flow configurations of the human vocal tract shown in Fig. 1 [8, 31] and the extended conical diffuser under study

Quantity	Symbol	Human vocal tract	Studied nozzle
Tube extension length	L_t	$0 \leq L_t \leq 19$ cm	$L_t \in \{3, 11, 18, 50\}$ cm
Nozzle outlet diameter	d	$0 \leq d \leq 3$ cm	$d = 2.5$ cm
Length-to-diameter ratio	L_t/d	$0 \leq L_t/d \leq 20$	$1.2 \leq L_t/d \leq 20$
Bulk Reynolds number	Re_b	$Re_b < 10^4$	$Re_b < 10^4$

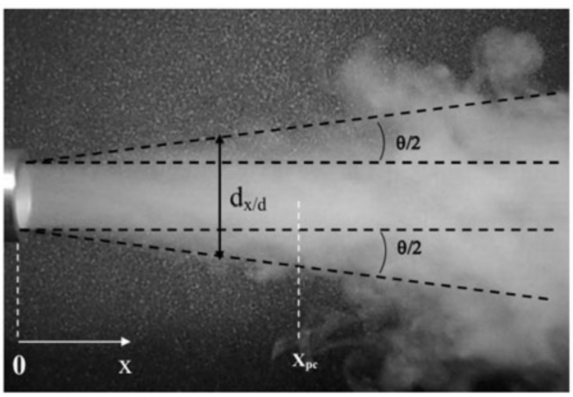

Fig. 3 Smoke visualisation of round jet flow development downstream from the extended conical diffuser nozzle with jet width $d_{x/d}$, total jet development angle θ and potential core extent x_{pc}

stages accuracy of positioning is 4 µm in the longitudinal, x, direction and 2 µm in the transverse, y, direction. Longitudinal velocity data along the centreline $y = 0$ are gathered from the tube exit $x/d = 0$ up to $x/d = 20$ with a longitudinal spatial step $\Delta x = 1$ cm, i.e. $\Delta x/d = 0.4$. Initial transverse velocity profiles are gathered with a transverse spatial step $\Delta y = 10^{-4}$ m at a longitudinal distance $x/d \leq 0.04$ from the nozzle exit. Velocity profiles are measured for different volume flow rates Q_b and length-to-diameter ratios L_t/d.

At each measurement position instantaneous velocity data are sampled at 40 kHz during 4 s consecutively. Statistical quantities are calculated from instantaneous velocity measurements to which a 10 kHz low pass filter is applied. The mean centreline velocity $U_c(x)$ and local centreline turbulence level u are calculated at each measurement position from the instantaneous velocities $U_{c,p}$ with subscript p indicating the pth instantaneous velocity sample. The turbulence level u is given as the root mean square of the centreline velocity:

$$u = \sqrt{\frac{1}{N_{tot}} \sum_{p=1}^{N_{tot}} (U_{c,p} - U_c)^2}, \tag{2}$$

in which N_{tot} denotes the total number of instantaneous velocity samples. The local centreline turbulence intensity u/U_c is defined as the ratio between the local centreline turbulence level u and the local mean centreline velocity U_c. Uncertainties on mean velocity U_c and local turbulence intensities u/U_c are estimated as < 1 % for $1.4 < U_{c,p} < 10$ m/s and < 5 % for $0.2 < U_{c,p} < 1.4$ m/s [13].

Table 2 Evolution of the initial mean streamwise centreline velocity U_0 for experimentally assessed bulk Reynolds numbers Re_b and length-to-diameter ratios $L_t/d = \{1.2, 4.4, 7.2, 20\}$. The corresponding ratios of the nozzle length to the diffusers throat diameter, $L_N/d_{in} = \{120, 280, 420, 1060\}$, are indicated as well

Re_b	1132	2264	3395	4527	5659	6791	7357	7922	8488	9054
U_b [m/s]	0.6	1.4	2.0	2.6	3.4	4.1	4.5	4.7	5.1	5.5
$L_t/d = 1.2$, $L_N/d_{in} = 120$										
U_0 [m/s]	1.9	2.7	3.6	4.5	5.5	6.3	6.8	7.6	8.0	8.4
$L_t/d = 4.4$, $L_N/d_{in} = 280$										
U_0 [m/s]	1.0	1.8	2.7	3.5	4.4	5.3	5.9	6.1	6.6	7.2
$L_t/d = 7.2$, $L_N/d_{in} = 420$										
U_0 [m/s]	1.1	1.9	2.8	3.7	4.7	5.7	6.3	6.6	7.1	7.7
$L_t/d = 20$, $L_N/d_{in} = 1060$										
U_0 [m/s]	1.3	2.2	3.1	4.1	5.1	6.1	6.7	7.0	7.6	8.2

4 Centreline velocity data

For all assessed nozzle extension lengths L_t/d, centreline velocity data are measured for 10 volume flow rates, which vary in the range $3 \times 10^{-4} \leq Q_b \leq 27 \times 10^{-4}$ m^3/s. The corresponding bulk Reynolds numbers at the nozzle exit Re_b,

$$Re_b = \frac{U_b d}{\nu}, \tag{3}$$

yield $1100 < Re_b < 10^4$ where U_b denotes the bulk velocity at the nozzle exit assuming an ideal fluid with uniform transverse velocity profile $U(y) = U_b$. The resulting range of Reynolds numbers $Re_b < 10^4$ is in accordance with values observed for flow through the human vocal tract as summarised in Table 1.

The influence of the upstream diffuser and applied length-to-diameter ratio L_t/d on flow development is outlined. The initial mean centreline velocity at the nozzle exit U_0 is discussed in Sect. 4.1. The measured centreline profiles are qualitatively dealt with in Sect. 4.2.

4.1 Initial mean centreline velocity at the nozzle exit

The measured initial mean centreline velocities at the nozzle exit U_0 vary in the range $1 \leq U_0 \leq 9$ m/s. Associated initial Reynolds numbers Re_0,

$$Re_0 = \frac{U_0 d}{\nu}, \tag{4}$$

are comprised between $1600 < Re_0 < 14100$. An overview of assessed initial conditions, Re_0 and U_0 as function of $(Re_b, L_t/d)$, is given in Table 2 for all assessed extension tube lengths L_t/d. The tube extension length L_t/d is seen to influence the initial mean centreline velocity at the tube exit U_0 to a large extent suggesting different mechanisms governing jet development as the extension tube length is varied.

Although the present paper focuses on the centreline velocity profiles, normalised initial mean transverse velocity profiles at the nozzle exit are considered in order to inform on flow development at the nozzle exit. Transverse profiles are illustrated in Fig. 4. Measured transverse profiles are compared to three well known transverse profiles: a theoretical uniform velocity profile $U(y) = U_0$ corresponding to a top-hat profile with vanishing momentum thickness, a parabolic profile corresponding to fully developed pipe flow and a 1/7 power law profile describing turbulent pipe flow [3, 30].

4.1.1 $L_t/d > 1.2$

For $L_t/d \in \{4.4, 7.2, 20\}$ or $280 \leq L_N/d_{in} \leq 1060$ the initial mean transverse velocity profiles shown in Fig. 4(a) for $Re_b = 1132$, Fig. 4(b) for $Re_b = 4527$ and Fig. 4(c) for $L_t/d = 20$ are observed to tend towards a parabolic profile as both the length-to-diameter L_t/d increases and the Reynolds number Re_b decreases. The observed evolution of the transverse profiles illustrates that the flow is characterised

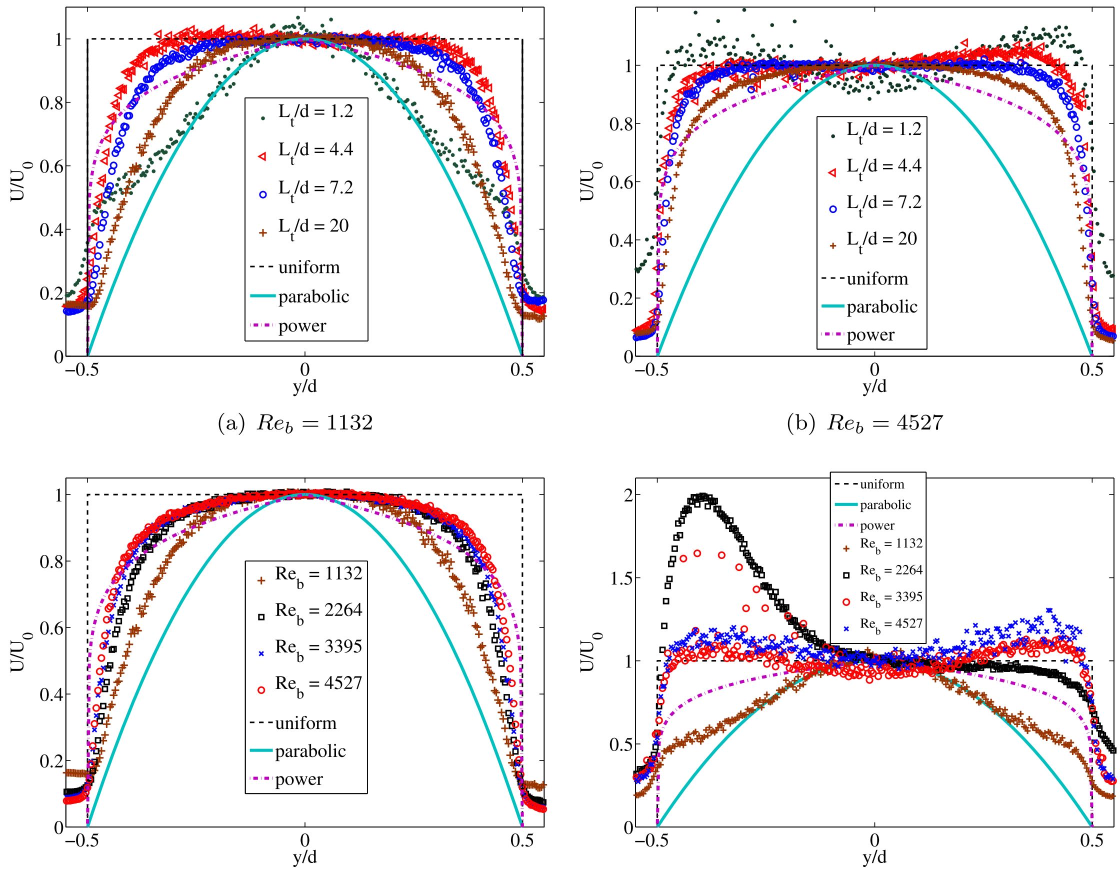

(a) $Re_b = 1132$ (b) $Re_b = 4527$

(c) $L_t/d = 20$ (d) $L_t/d = 1.2$

Fig. 4 Illustration of initial mean transverse velocity profiles normalised by the mean initial centreline velocity measured at $x/d < 0.04$, $U(y)/U_0$. Typical profiles measured for (**a**) $Re_b = 1132$, (**b**) $Re_b = 4527$, (**c**) $L_t/d = 20$ and (**d**) $L_t/d = 1.2$ are shown. As a reference a theoretical uniform velocity profile $U(y) = U_0$ corresponding to a top-hat profile with vanishing momentum thickness (*uniform*), a parabolic profile corresponding to fully developed pipe flow (*parabolic*) and a 1/7 power law profile describing turbulent pipe flow (*power*) are depicted as well

by partial pipe flow development in the extension tube. No fully developed pipe flow is observed due to the limited length-to-diameter ratio $L_t/d \leq 20$ which is much smaller than the value of 40 associated with fully developed pipe flow [3, 30]. Instead, the profiles exhibit a uniform centre portion and reduced velocity in the vicinity of the wall. Therefore, the measured profiles correspond to top-hat profiles for which the momentum thickness increases as the uniform centre portion narrows, i.e. for increasing length-to-diameter L_t/d and decreasing Reynolds number Re_b. For a constant length-to-diameter ratio L_t/d, profiles for Reynolds number $Re_b \geq 4527$ almost collapses. Consequently, for $L_t/d \geq 4.4$ or $L_N/d_{in} \geq 280$ the presence of the upstream diffuser leaves no particular imprint on the initial transverse flow profiles which are governed by boundary layer development in the uniform tube extension.

4.1.2 $L_t/d = 1.2$

From Table 2 it is seen that the initial mean centreline velocities U_0 observed for $L_t/d = 1.2$ exceed the values measured for $L_t/d > 1.2$ regardless the assessed Reynolds numbers, Re_b. This discrepancy in mean initial centreline velocity U_0 suggests that the flow development through the extension tube for $L_t/d = 1.2$, corresponding to $L_N/d_{in} = 120$, is not governed by boundary layer developement as is the case for $L_t/d \in \{4.4, 7.2, 20\}$. Initial mean transverse velocity profiles

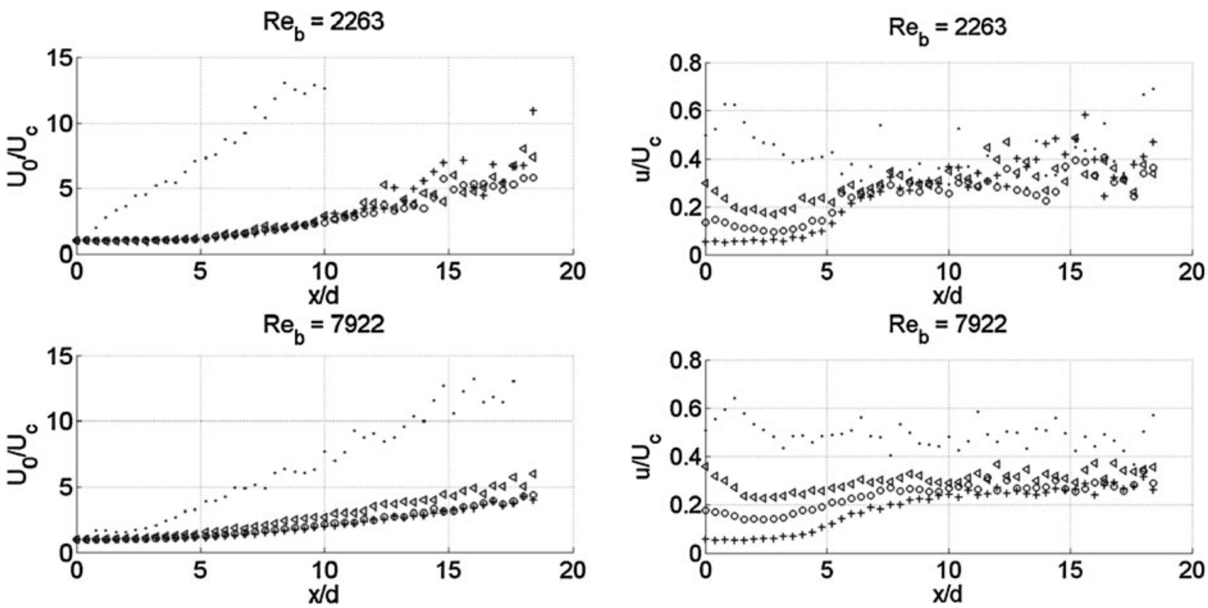

(a) mean $U_0/U_c(x)$

(b) turbulence intensity $u/U_c(x)$

Fig. 5 Illustration of (**a**) normalised centreline mean velocity profiles $U_0/U_c(x)$ and (**b**) local centreline turbulence intensity profiles u/U_c for bulk Reynolds numbers $Re_b \in \{2263, 7922\}$ and for all assessed length-to-diameter ratios $L_t/d = 1.2$ (•), $L_t/d = 4.4$ (◁), $L_t/d = 7.2$ (○), $L_t/d = 20$ (+)

for $L_t/d = 1.2$ illustrated in Fig. 4(d) show that the flow is determined by flow separation from the walls inside the divergent portion of the diffuser. As the Reynolds number is increased from $Re_b = 1132$ up to $Re_b = 4527$ the flow properties vary. For $Re_b = 1132$, the flow separates from the walls near the diffusers throat and proceeds as an axisymmetrical jet which develops in the conical extension so that the centre portion of the initial mean transverse velocity profile coincides with a parabolic velocity profile due to the large ratio $L_N/d_{in} = 120$ which is much greater than 40 [3, 30]. The side portions are dominated by flow entrainment and eddies surrounding the jet. As the Reynolds number is increased to $Re_b = 2264$ flow separation at the diffusers throat is not complete. Consequently, the proceeding jet is partly attached to the wall so that the jet develops not symmetrically along the centreline. Instead, the jet profile approximates the profile of a wall jet [30]. The measured mean centreline velocity U_0 yields about half the maximum velocity. As for $Re_b = 1132$ eddy formation and flow entrainment determines the velocity profile in the portion surrounding the jet. Further increasing the Reynolds number restores the symmetry of the mean transverse profile suggesting that no massive flow separation occurs. The overall profile is characterised by an overall unsteadiness which increases with increasing Reynolds number. The transverse profiles are further characterised by a small boundary layer in the wall vicinity next to a velocity overshoot due to flow entrainment. The same way as for $L_t/d > 1.2$, profiles for Reynolds number $Re_b \geq 4527$ almost collapses. Consequently, for $L_t/d = 1.2$ or $L_N/d_{in} = 120$ the presence of the upstream diffuser shapes the initial transverse flow profile.

Despite the revailed differences in underlying flow development and consequently in initial mean transverse velocity profiles, all length-to-diameter ratios L_t/d are reported on in the remainder of this manuscript, since all configurations are relevant with respect to the upper airways as illustrated in Fig. 1 and Table 1.

4.2 Centreline profiles: mean and turbulence intensity

Measured mean streamwise centreline velocity profiles $U_c(x)$ normalised by the initial mean centreline velocity U_0 and associated centreline turbulence intensities $u/U_c(x)$ are illustrated in Fig. 5 for all assessed length-to-diameter ratios L_t/d for $Re_b = 2263$

and $Re_b = 7922$. Since the initial mean centreline velocity U_0 revealed different governing jet development mechanisms for $L_t/d > 1.2$ and $L_t/d = 1.2$, centreline profiles for $L_t/d \in \{4.4, 7.2, 20\}$ and $L_t/d = 1.2$ are discussed separately.

4.2.1 $L_t/d > 1.2$

For length-to-diameter ratios $L_t/d > 1.2$, the mean centreline velocity, illustrated in Fig. 5(a), exhibits a potential core region downstream from the nozzle exit for all assessed Reynolds numbers. Inside the potential core region, the mean streamwise centreline velocity U_c approximates the initial mean streamwise centreline velocity U_0. Downstream from the potential core, the mean streamwise centreline velocity decays. The potential core extent and the mean centreline velocity decay depend on the imposed Reynolds number Re_b as well as on the length-to-diameter ratio L_t/d determining boundary layer development of the initial mean transverse profile. Thickening of the boundary layer, occurring as L_t/d increases or Re_b decreases as outlined in Sect. 4.1, increases jet stability so that the potential core extent increases.

The local turbulence intensities u/U_c are illustrated in Fig. 5(b). At the end of the potential core the surrounding mixing region collapses so that, for $L_t/d > 1.2$, the turbulence intensity increases until an asymptotic value of the turbulence intensity is reached (0.3–0.4). The asymptotic value depends on Reynolds number Re_b as well as on length-to-diameter ratio L_t/d. Inside the potential core the turbulence intensity increases as the length-to-diameter ratio L_t/d decreases and to a less degree as the Reynolds number Re_b increases. The length-to-diameter ratio determines the initial centreline turbulence intensity at the nozzle exit u_0/U_0. The initial centreline turbulence intensity at the nozzle exit, $x/d = 0$, increases from 7 % to 50 % as the length-to-diameter ratio decreases.

Consequently, although the initial mean centreline profile is mainly shaped by boundary layer development along the walls of the uniform extension tube, the initial turbulence intensity u_0/U_0 is determined due to flow instabilities induced downstream the diffuser throat accompanying the flow deceleration along the diffuser. The generated turbulent and mean flow motions are transported downstream towards the nozzle exit and influences the stability of the emitted jet. For $L_t/d = 20$ the turbulent intensity u/U_c is constant inside the potential core indicating the absence of turbulence production and the complete dissipation of flow motion produced along the diffuser. For $L_t/d = 7.5$ and $L_t/d = 4.4$ on the other hand the turbulence intensity inside the potential core decreases immediately downstream from the nozzle exit due to the ongoing dissipation of fluid motion. The loss of turbulence continues until the collapse of the mixing region becomes notable. Consequently, jet stability decreases as the extension length L_t reduces, even for $L_t/d > 1.2$.

4.2.2 $L_t/d = 1.2$

In the previous Sect. 4.1, it is argued that for $L_t/d = 1.2$ complete or partial flow separation along the diffuser walls introduces structures which influence the mean centreline velocity profile in the near region downstream the nozzle exit. In order to ensure that no large coherent structures occur, power spectra of the time velocity signal are computed at different downstream measurement locations $x/d \in \{1, 2, 3, 4, 5\}$. Power spectra of centreline velocity signals for $Re_b = 1132$ and $Re_b = 4527$ are shown in Fig. 6. No sharp frequency peaks or humps are observed so that it is concluded that the mean centreline velocity profile is not affected by the passage of large coherent structures in the near field downstream from the tube exit. It is seen from Fig. 6 that the bandwidth of the power spectra increases with Reynolds number Re_b which corresponds to the increase in turbulence intensity with Reynolds number Re_b observed from Fig. 5(b).

Figure 5(a) shows that the potential core region associated with $L_t/d = 1.2$ is reduced compared to values observed for length-to-diameter ratios $L_t/d > 1.2$. In addition, the Reynolds number dependence is enhanced since the extent of the potential core x_{pc} decreases quickly with the Reynolds number Re_b. The potential core region vanishes for low Reynolds numbers $Re_b \leq 2264$ for which jet formation at the throat of the diffuser is observed as outlined in Sect. 4.1. Consequently, the near field downstream the nozzle exit corresponds to the decay portion of the jet formed at the diffusers throat so that no potential core is observed. For Reynolds numbers $Re_b > 2264$, the mean centreline velocity inside the potential core reduces immediately downstream from the nozzle exit up to $x/d \approx 1.3$ followed by a constant velocity region as observed in case of jet forcing. This first velocity reduction is limited to approximately 1 % at $x/d \approx 1.3$.

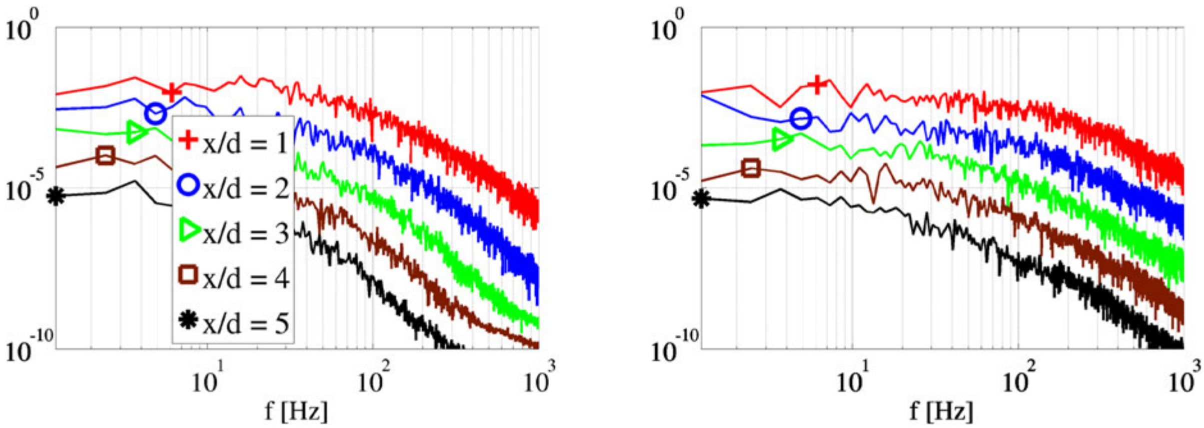

(a) $Re_b = 1132$ and $L_t/d = 1.2$ (b) $Re_b = 4527$ and $L_t/d = 1.2$

Fig. 6 Power spectra of centreline velocity signals for $L_t/d = 1.2$ for (**a**) $Re_b = 1132$ and (**b**) $Re_b = 4527$ at five downstream positions $x/d = 1$ (+), $x/d = 2$ (○), $x/d = 3$ (▹), $x/d = 4$ (□) and $x/d = 5$ (∗). Every spectrum is shifted downwards with respect to the previous

Downstream from the potential core, the centreline velocity decays more quickly than observed for $L_t/d > 1.2$ due to the flow instability and the breakdown of the small structures. Since the flow instability depends on Reynolds number Re_b, the rate of centreline velocity decay varies with Reynolds number Re_b. Consequently, proximity of the upstream diffuser decreases jet stability and therefore it favours centreline velocity decay.

Figure 5(b) illustrates the initial turbulence intensity at the nozzle exit for $L_t/d = 1.2$. The initial turbulence intensity at the nozzle exit yields 50 % regardless the Reynolds number Re_b due to the presence of small eddies. Immediately downstream from the nozzle exit flow entrainment increases the turbulence intensity until a maximum is reached. Further downstream the turbulence intensity reaches an asymptotic value. Note that due to the high turbulence intensity the measurement error on reported values is amplified.

5 Mean centreline velocity characterisation

In the following, the mean centreline velocity decay U_0/U_c outside the potential core and potential core extent x_{pc} are quantified.

5.1 Mean centreline velocity decay

Modelling of the mean streamwise centreline velocity U_0/U_c as a self-similar axisymmetric jet is assessed. The linear dependency on x/d characterises the jet in the self-similar portion and is commonly expressed by the decay equation given in (1) [19]. Consequently, the mean centreline velocity behaviour in the decay portion of the jet is characterised by evaluation of the least-square regression coefficients, i.e. decay constant $K(U_0)$ and virtual origin x_0, from the measured centreline velocity data.

The regression interval to estimate velocity decay constant $K(U_0)$ and virtual origin x_0 is typically $10 < x/d < 20$. The exact value of the lower limit of the regression interval depends on the Reynolds number Re_b. The lower limit of the regression interval, $x/d \approx 10$, is situated farther upstream than values commonly reported in literature for convergent nozzles such as $x/d \approx 16$ mentioned in [19]. The upstream shift of the regression interval is due to the presence of the diffuser which perturbs the flow as observed from the increased turbulence intensities compared to convergent nozzles. The current interval is in accordance with the regression interval used in [29, 32] and with the interval used in case a perturbation is due to an upstream abrupt contraction instead of an upstream diffuser [13].

Resulting regression coefficients, $K(U_0)$ and x_0, are summarised in Table 3 as function of bulk Reynolds number Re_b and length-to-diameter ratio L_t/d. The spatial accuracy of the measurement positions along the centreline $\Delta x/d = 0.4$, indicated in Sect. 3, allows an accurate estimation of regression parameters despite the limited extent of the regression interval. Es-

Table 3 Estimated virtual origin x_0 and velocity decay rate $K(U_0)$ for assessed bulk Reynolds numbers Re_b and length-to-diameter ratio $L_t/d = \{1.2, 4.4, 7.2, 20\}$

Re_b	1132	2264	3395	4527	5659	6791	7357	7922	8488	9054
$L_t/d = 1.2$										
x_0 [m]	0.15	0.15	0.06	0.02	0.04	0.02	0.02	0.03	0.02	0.03
K	0.11	0.3	1.2	1.3	1.1	1.3	1.4	1.2	1.2	1.3
$L_t/d = 4.4$										
x_0 [m]	0.14	0.09	0.07	0.02	0.04	0.02	0.01	0.02	0.02	0.02
K	0.5	3.3	2.7	3.2	3	3.4	3.6	3.3	3.4	3.3
$L_t/d = 7.2$										
x_0 [m]	0.18	0.09	0.05	0.04	0.04	0.04	0.02	0.02	0.02	0.02
K	0.8	2.6	3.6	3.7	3.9	4	4.2	4.4	4.5	4.3
$L_t/d = 20$										
x_0 [m]	0.19	0.13	0.1	0.04	0.06	0.05	0.03	0.04	0.04	0.04
K	0.5	1.6	2.5	4.3	4	4.2	4.4	4.4	4.1	4.2

timated values of $K(U_0)$ as function of the mean centreline velocity at the tube exit are shown in Fig. 7(a). An overview of values reported in literature is given in Table 4.

For all assessed length-to-diameter ratios L_t/d the decay coefficient $K(U_0)$ increases with U_0 whereas the virtual origin x_0 decreases. The found tendencies are consistent with observations reported for convergent nozzles at bulk Reynolds numbers $7000 < Re_b$ [19]. Nevertheless, estimated decay coefficients $K(U_0) \leq 4.2$ are smaller than $K > 5$ typically reported for high Reynolds number flow as seen from Table 4. This is again in agreement with findings reported for moderate Reynolds numbers $7000 < Re_b$ for convergent nozzles [19].

The $K(U_0)$ data presented in [19] collapse almost on a single curve regardless the used nozzle exit diameter $4 \leq d \leq 15$ cm as schematically shown in Fig. 7(a). The $K(U_0)$ curve increases for low velocities $U_0 < 6$ m/s in the range $3.8 < K(U_0) \leq 6.22$ and is almost constant $K(U_0) \approx 6$ for moderate velocities $U_0 > 6$ m/s. From Fig. 7(a) is seen that although for increased U_0 an increase of $K(U_0)$ is indeed followed by an almost constant portion for all assessed length-to-diameter ratios L_t/d, the shape of the curves differs as function of the used length-to-diameter ratio L_t/d so that no longer a single curve is obtained describing $K(U_0)$ for all assessed length-to-diameter ratios L_t/d, instead $K(U_0, L_t/d)$ holds. Nevertheless, a threshold mean centreline velocity $U_0 \approx 4.5$ m/s can be associated with the onset of a constant $K(U_0)$ value, which is lower than $U_0 \approx 6$ m/s observed on a convergent nozzle [19]. The numerical value of $K(U_0)$ in the constant portion of the curve $K(U_0)$ for $U_0 \geq 4.5$ m/s as well as the shape of the increasing curve portion for $U_0 < 4.5$ m/s depends on the applied length-to-diameter ratio L_t/d.

In Sect. 4, it is argued that the applied length-to-diameter ratio L_t/d influences flow development mainly governed by boundary layer growth in the extension tube for $L_t/d > 1.2$ and by flow separation downstream the diffusers throat for $L_t/d = 1.2$. Therefore, the found dependence of the decay coefficient $K(U_0)$ on the used length-to-diameter ratio L_t/d reflects differences in centreline decay associated with different jet flow development. For $L_t/d = 1.2$, flow separation along the diffuser walls results in jet formation or flow instabilities, which favour velocity decay so that $K(U_0)$ is decreased compared to values associated with $L_t/d > 1.2$. For $L_t/d > 1.2$ the high initial flow turbulence intensities indicate the presence of small scale turbulence structures which limit flow entrainment and hence centreline velocity decay. Nevertheless, the size of the flow structures is influenced by the length-to-diameter ratio L_t/d as shown by the difference in initial centreline turbulence intensity and its centreline evolution. As the initial centreline turbulence intensity decreases the centreline ve-

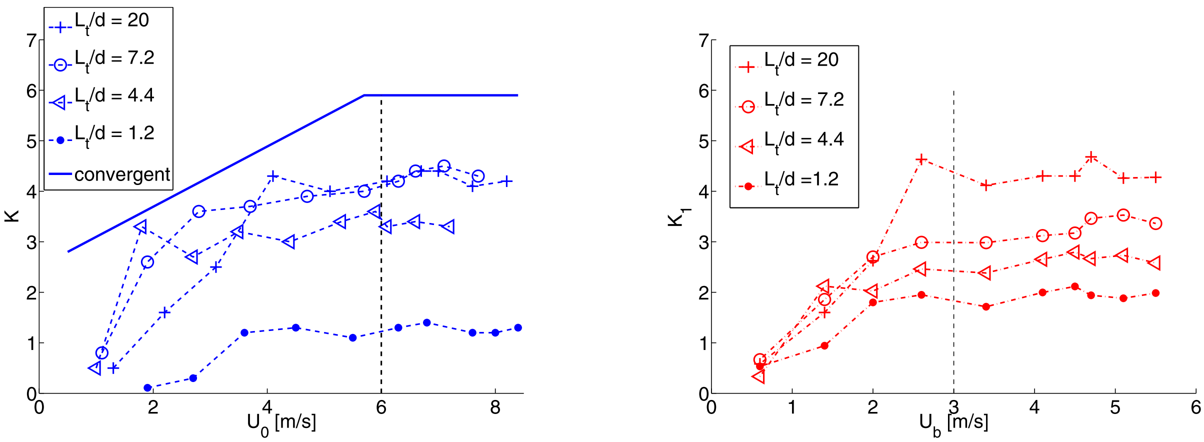

(a) $K(U_0)$ (b) $K_1(U_b)$

Fig. 7 Velocity decay constant (**a**) $K(U_0)$ and (**b**) $K_1(U_b)$ for $L_t/d = 1.2$ (•), $L_t/d = 4.4$ (◁), $L_t/d = 7.2$ (○), $L_t/d = 20$ (+). As a benchmark $K(U_0)$ tendency reported for a convergent nozzle [19] are added in Fig. 7(a) (*convergent*). The *vertical dashed line* indicates $U_0 = 6$ m/s which is reported as a threshold velocity in [19] so that for $U_0 > 6$ m/s K remains constant. In Fig. 7(b) the *vertical dashed line* indicates the threshold velocity $U_b = 3$ m/s so that for $U_b > 3$ m/s K_1 can be approximated by a constant. Note that in this case the constant depends on the used length-to-diameter ratio L_t/d

Table 4 Comparison of centreline mean velocity coefficients x_0/d and K of current and previous studies of round free jets

	nozzle	Re_b	x_0/d	K
Wygnanski et al. [33]	convergent	10^5	3	5.7
Panchapakesan et al. [24]	convergent	1.1×10^4	−2.5	6.06
Mi et al. [22]	convergent	1.6×10^4	3.5	4.48
	long pipe	1.6×10^4	4.73	4.64
Xu et al. [34]	convergent	8.6×10^4	3.7	5.6
	long pipe	8.6×10^4	2.6	6.5
Hussein et al. [17]	convergent	9.5×10^4	4	5.8
Fellouah et al. [10]	convergent	3×10^4	2.5	5.59
Quinn [26]	convergent	1.84×10^5	2.15	5.99
Malmström et al. [19]	convergent	$6500 \le Re_b \le 9.7 \times 10^4$	$-0.3 \le x_0/d \le 4.0$	$3.8 \le K \le 6.22$
current	extended diffuser	$1132 \le Re_b \le 9054$	$0.02 \le x_0/d \le 0.19$	$0.11 \le K \le 4.5$

locity decay decreases as well, corresponding to increased values of $K(U_0)$. Consequently, for a fixed mean centreline velocity U_0, a decrease of the length-to-diameter ratio L_t/d results in an increase of the turbulence intensity and therefore in a decrease of the decay parameter K. The described flow development and its influence on the estimated decay coefficient K is in agreement with the evolution of $K(U_0)$ described in [32] for a single bulk Reynolds number.

The current data suggest that for moderate initial turbulence intensities $u_0/U_0 < 20$ % and for $U_0 > 4.5$ m/s, i.e. $L_t/d \ge 7.2$, K and U_0 can be correlated in a single way regardless the used length-to-diameter ratio L_t/d. The found turbulence level $u_0/U_0 < 20$ % confirms findings reported in [19, 23] for a convergent nozzle where increasing the turbulence intensity from 4 to 10 % did not alter the decay coefficient K. Although, a functional relationship $K(U_0)$ is shown not to hold for high turbulence intensities, $u/U_c > 20$ %,

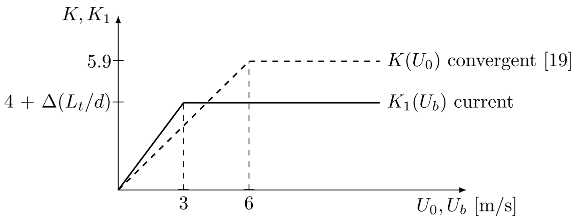

Fig. 8 Summary of asymptotic behaviour of decay coefficient $K(U_0)$ for a convergent nozzle [19] and decay coefficient $K_1(U_b)$ for the extended conical diffuser under study

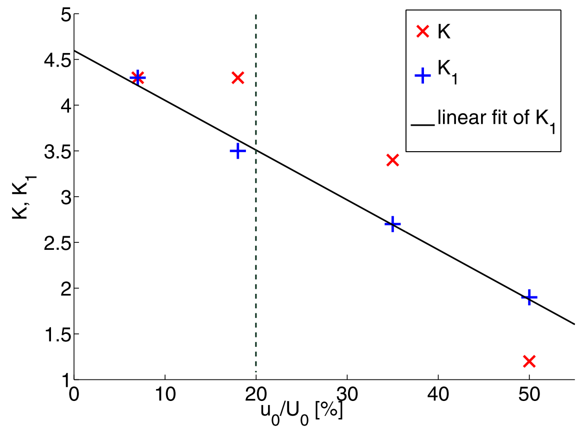

Fig. 9 Asymptotic velocity decay constants K (×) and K_1 (+) as function of initial streamwise turbulence intensity u_0/U_0 which yields 7, 18, 35 and 50 % for L_t/d equal to 20, 7.2, 4.4 and 1.2, respectively. The *vertical dashed line* corresponds to an initial centreline turbulence intensity $u_0/U_0 = 20$ % below which the decay constant K approximates a constant value. In addition, the linear approximation $K_1 \approx -0.052 \times u_0/U_0 + 4.5$ is plotted (*full line*)

due to shortening of the extension length L_t/d or due to increasing the Reynolds number Re_b. Therefore another expression is sought to compensate for the differences in flow development expressed by differences in initial mean transverse velocity profiles at the nozzle exit or by differences in centreline turbulence intensities. The variation of initial mean transverse velocity data leads to the broad range of initial mean centreline velocity values U_0 associated with a single bulk Reynolds number Re_b and hence a single bulk velocity U_b. Therefore, it is proposed to insert the ratio U_0/U_b in Eq. (1) describing the mean centreline velocity decay $U_c(x)$ resulting in an expression correlating $U_c(x)$ to the bulk velocity U_b as:

$$\frac{U_c(x)}{U_b} = K_1 \frac{d}{x - x_0}, \tag{5}$$

in which $K_1(U_b) = \frac{U_0 K}{U_b}$ provides an alternative decay constant to $K(U_0)$.

Resulting alternative decay coefficients $K_1(U_b)$ are illustrated in Fig. 7(b). As for $K(U_0)$, the decay constant $K_1(U_b)$ is seen to decrease steeply from an approximately constant value for $U_b < 3$ m/s for all assessed length-to-diameter ratios. Consequently, a single threshold value $U_b \approx 3$ m/s is found in order to describe the asymptotic decay behaviour using Eq. (5). Approximate constant $K_1(U_b)$ values are seen to decrease for decreasing L_t/d ratio, indicating that no single asymptotic value is reached as observed for $K(U_0)$ for low initial turbulence intensities measured for $L_t/d \geq 7.2$ and $U_0 > 4.5$ m/s or as observed for a convergent nozzle for $U_0 > 6$ m/s [19]. A schematic overview of $K(U_0)$ and $K_1(U_b)$ is given in Fig. 8.

The values for $K(U_0 > 4.5$ m/s) and $K_1(U_b > 3$ m/s) associated with the constant portion in Fig. 7 are correlated with the initial centreline turbulence intensity at tube outlet u_0/U_0, i.e. $u_0/U_0 \in \{7, 18, 35, 50\}$ % for $L_t/d \in \{20, 7.2, 4.4, 1.2\}$. Resulting $K(u_0/U_0)$ and $K_1(u_0/U_0)$ are shown in Fig. 9. The self-similar behavior for $K(U_0)$ resulting in $K(U_0) \approx 4.3$ is observed for $U_0 > 4.5$ m/s and $u_0/U_0 < 20$ %.

Furthermore, current data suggest that the relationship $K_1(u_0/U_0)$ can be approximated by a linear *ad-hoc* relationship $K_1(U_b)$,

$$K_1\left(\frac{u_0}{U_0}\right) \approx -0.052 \times \frac{u_0}{U_0} + 4.5, \tag{6}$$

to within 5 %. Consequently, expressing the decay relationship as function of U_b rather than U_0 allows to approximate the decay coefficient K_1 by using the proposed linear relationship as function of the initial centreline turbulence intensity regardless the length-to-diameter ratios L_t/d. The mean centreline velocity decay for $U_b > 3$ m/s is than given by Eq. (5) for both $L_t > 1.2$ and for $L_t = 1.2$ despite the outlined differences in flow development mechanisms. This is not the case when expressing the decay as function of U_0 following Eq. (1).

5.2 Potential core extent

The potential core extent x_{pc} is defined as the abscissa corresponding to the intersection point of the line $U_c(x) = U_0$ with the extrapolated decay portion of the mean centreline velocity discussed in the previous section [29]. Application of this definition of

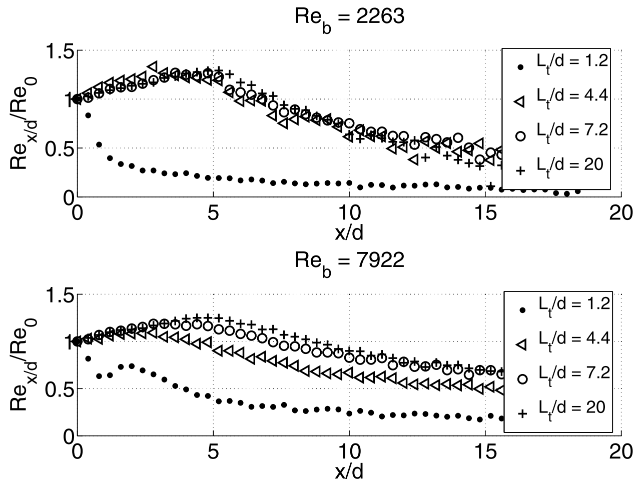

Fig. 10 Evolution of the normalised local Reynolds number $Re_{x/d}/Re_0$ at $Re_b = 2263$ and $Re_b = 7922$ for $L_t/d = 1.2$ (•), $L_t/d = 4.4$ (◁), $L_t/d = 7.2$ (○), $L_t/d = 20$ (+)

the potential core extent requires *a-priori* knowledge of the mean centreline velocities. Moreover, applying this definition lacks robustness since e.g. jet forcing or the passage of large coherent structures might cause $U_c(x) \neq U_0$ upstream from the end of the potential core for $x < x_{pc}$. The same drawbacks can be formulated for derived threshold based definitions such as $U_c(x = x_{pc}) \geq p \times U_0$ with p indicating a fixed ratio of U_0, e.g. $p = 0.95$ [2].

A second approach to estimate the potential core extent x_{pc} consists in applying the definition $U_c(x = x_{pc}) \geq U_0$ to the decay model presented in Eq. (1) instead of to the measured mean centreline velocity data. This results in the following expression for x_{pc}:

$$\frac{x_{pc} - x_0}{d} = K. \tag{7}$$

It is seen from Eq. (7) that the potential core extent x_{pc} can only be determined in case the decay coefficient K and virtual origin x_0 are known so that the drawback of *a-priori* knowledge is not eliminated. Note that the same remark holds in case the alternative decay relationship Eq. (5) is used requiring *a-priori* knowledge of K_1 and x_0.

A third alternative x_{pc} estimation is derived assuming a Gaussian transverse velocity profile of the jet and streamwise constant momentum [19]. The total jet spreading angle θ, depicted in Fig. 3, becomes than:

$$\tan\frac{\theta}{2} = \frac{\sqrt{0.5 \ln 2}}{K_w}, \tag{8}$$

where K_w denotes a transverse centreline decay coefficient. A local Reynolds number $Re_{x/d}$ along the centreline is defined as

$$Re_{x/d} = \frac{U_c(x/d) \times d_{x/d}}{\nu} \tag{9}$$

where $U_c(x/d)$ denotes the measured mean streamwise local centreline velocity and $d_{x/d}$ the local jet width as depicted in Fig. 3. The local jet width $d_{x/d}$ is easily estimated from the jet spreading angle θ following Eq. (8) as $d_{x/d} = 2\frac{x}{d} \times \tan\frac{\theta}{2} + d$. Note that the jet spreading angle θ determines the decay constant K_w following Eq. (8).

The local Reynolds number $Re_{x/d}$ exhibits a maximum at $x = x_{\max}$ along the centreline. The occurrence and position of a maximum is easily understood since on one hand the local jet width $d_{x/d}(x)$ increases downstream from the nozzle exit whereas on the other hand the mean centreline velocity is almost constant $U_c \sim U_0$ inside the potential core $x \leq x_{pc}$ and decreases $U_c < U_0$ downstream from the potential core extent $x > x_{pc}$. The evolution of the local Reynolds number $Re_{x/d}$ and the occurrence of a maximum is illustrated in Fig. 10 for $Re_b = 2263$ and $Re_b = 7922$ for all assessed length-to-diameter ratios L_t/d. A maximum at the nozzle exit $x = 0$, such as occurring for $L_t/d = 1.2$, is interpreted as the absence of a potential core as is indeed the case for $L_t/d = 1.2$ as discussed in Sect. 4.

The position $x_{\max}$ of the local Reynolds number $Re_{x/d}$ depends on the spreading angle θ. Increas-

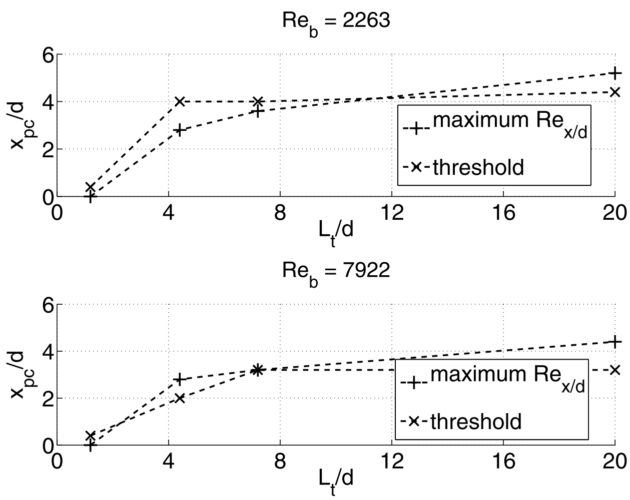

Fig. 11 Comparison of the estimated position of the end of the potential core x_{pc} obtained with the maximum Reynolds criterion for $\theta = 4.5°(+)$ and with the threshold criterion for $p = 0.95$ (×) for $Re_b = 2263$ and $Re_b = 7922$

Table 5 Overview of empirical criteria in order to predict the potential core extent x_{pc}

Procedure	Criteria	Required data	Major drawback	Major advantage
threshold	$U_c(x = x_{pc}) \geq p \times U_0$ with $0.9 \leq p \leq 1$	mean centreline velocities $U_c(x)$	– not robust – $U_c(x)$ data or modelled data (Eq. (5) and Eq. (6))	simple
decay	$x_{pc} = K_{(1)}d + x_0$	$U_c(x)$ + estimation of $K_{(1)}$ and x_0	asymptotic values $K_{(1)}$ and x_0 are not unique for $U_b < 3$ m/s % and $u_0/U_0 > 20$ %	use of asymptotic x_0 and $K(U_0)$ or $K_1(U_b)$
maximum Reynolds	$Re_{x_{\max}/d} = \max(Re_{x/d})$ with $\theta = 4.5°$	$U_c(x)$	$U_c(x)$ data or modelled data (Eq. (5) and Eq. (6))	robust

ing θ results in a downstream shift of $x_{\max}$ regardless Reynolds number Re_b and length-to-diameter ratio L_t/d. The local maxima associated with a constant total spreading angle $\theta = 4.5°$ in accordance with the spreading angle expected for a turbulent jet [30], i.e. $K_w = 14$ following Eq. (8), provides an approximation of the potential core extent for all assessed Re_b and L_t/d so that $x_{\max}(\theta = 4.5°) \approx x_{pc}$ holds. Figure 11 compares estimations of the potential core extent x_{pc} obtained with a threshold criterion $U_c(x = x_{pc}) \geq 0.95U_0$ and obtained with the maximum Reynolds number criterion $x_{\max}(\theta = 4.5°) \approx x_{pc}$.

Both estimations of the potential core extent x_{pc} agree to within twice the longitudinal spatial step in the measurement, i.e. $\Delta x/d = 0.4$. The potential core extent increases as the length-to-diameter ratio L_t/d increases and decreases as the Reynolds number Re_b increases as qualitatively discussed in Sect. 4.2. The $x_{\max}$ criterion predicts the absence of a potential core i.e. $x_{pc} = 0$ for $L_t/d = 1.2$. Therefore, $x_{\max}$ obtained with a total spreading angle $\theta = 4.5°$ provides an alternative criterion to estimate the potential core, at least for the Re_b range and L_t/d range under study.

A summary of different criteria is given in Table 5. Note that measured mean centreline velocities $U_c(x)$ can be replaced by modelled centreline velocities in case $U_b > 3$ m/s holds, by using the decay relationship given in Eq. (5) and the linear relationship $K_1(U_b)$ given in Eq. (6) so that no centreline measurements are required. Obtained values of x_{pc} matches to within 1 %.

Table 6 Empirical asymptotic values averaged for $Re_b \geq 5659$ of the potential core extent x_{pc}/d and velocity decay coefficient K as function for length-to-diameter ratios $L_t/d = \{1.2, 4.4, 7, 2, 20\}$

L_t/d	1.2	4.4	7.2	20
x_{pc}/d	0	2.8	3.8	4.4
K	1.3	3.2	4	4

5.3 Mean centreline velocity modelling

The decay behaviour and potential core extent outlined in the previous section are applied in order to model the centreline mean velocity by applying the decay equation given in Eq. (1). For each assessed length-to-diameter ratio L_t/d the values for the potential core extent x_{pc} and asymptotic decay coefficients $K(U_0)$ obtained for $Re_b \geq 5659$ are averaged. Resulting values as function of length-to-diameter ratio L_t/d are summarised in Table 6.

The values of x_{pc} and K given in Table 6 are applied to model the mean centreline velocity $U_c(x)$ for a known outlet centreline velocity U_0 and length-to-diameter ratio L_t/d. Consequently, K and x_{pc} are used as constant model parameters for all assessed length-to-diameter ratios L_t/d and Reynolds numbers Re_b.

Furthermore, inside the potential core $x \leq x_{pc}$ the mean centreline velocity is assumed to remain constant so that $U_c(x \leq x_{pc}) = U_0$ holds. Downstream from the potential core $x > x_{pc}$ the mean streamwise velocity decay is modelled following Eq. (1). In order to apply Eq. (1) the decay coefficient K and virtual origin x_0 need to be known. The decay coefficient K is set to the constant value given in Table 6 so that K depends only on L_t/d and not on the initial mean centreline velocity U_0. The virtual origin x_0 follows immediately from Eq. (7) as $x_0 = x_{pc} - Kd$.

The simplified model of the mean centreline velocity is applied to all bulk Reynolds numbers using empirical asymptotic constant values for the model coefficients K and x_{pc}. Modelled and measured mean centreline velocities are illustrated in Fig. 12(a) for $Re_b = 2263$ and in Fig. 12(b) for $Re_b = 7922$. Despite the simplicity of the model approach, the overall model error smaller than 10 %. Despite the assumption of constant model coefficients derived for $Re_b \geq 5659$ no increase in model error is found when the model is applied to $Re_b < 5659$. In addition, the model can be applied to data obtained for extension lengths $L_t/d = 1.2$ as well as $L_t/d > 1.2$. Consequently, the outlined model provides a simple estimation of the centreline velocity decay in case of extended conical diffusers with length-to-diameter ratio $1.2 \leq L_t/d \leq 20$ and moderate Reynolds numbers $Re_b < 10^4$.

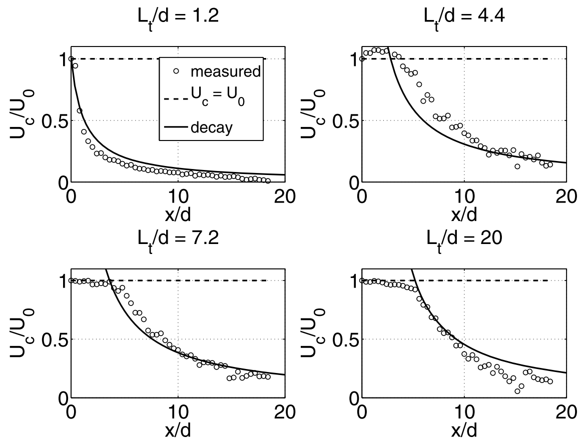

(a) $Re_b = 2263$

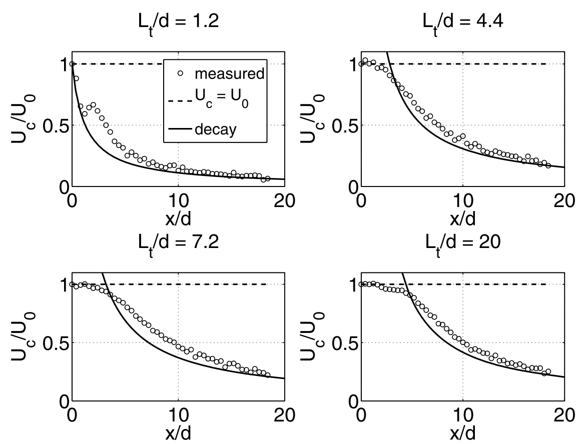

(b) $Re_b = 7922$

Fig. 12 Comparison of the measured normalised mean centreline velocity U_c/U_0 (○) at (**a**) $Re_b = 2263$ and (**b**) $Re_b = 7922$ for $L_t/d = \{1.2, 4.4, 7.2, 20\}$ with $U_c/U_0 = 1$ for $x \leq x_{pc}$ (*dashed line*) and Eq. (1) for $x > x_{pc}$ using K and x_{pc} values summarised in Table 6 (*solid line*)

6 Conclusion

The mean streamwise centreline velocity of an axisymmetrical jet issuing from an extended diffuser is experimentally studied for low length-to-tube diameter ratios $1.2 < L_t/d < 20$ and for moderate bulk Reynolds numbers $Re_b < 10^4$. The following conclusions are made:

- For $L_t/d = 1.2$ the mean transverse velocity profile at the nozzle outlet is governed by complete or partial flow separation along the walls of the diffuser. For $L_t/d > 1.2$ the mean transverse velocity profile is mainly governed by boundary layer growth in the uniform tube extension of length L_t. Moreover decreasing the extension tube increases the initial centreline turbulence intensity u_0/U_0 due to the presence of the upstream diffuser.
- Decreasing the extension tube decreases the mean streamwise centreline velocity decay constant $K(U_0)$. It is shown that no single asymptotic value of $K(U_0)$ is reached in case the initial streamwise turbulence intensity $u_0/U_0 > 20$ %.
- An asymptotic value of the mean centreline velocity decay coefficient, expressed as function of the bulk velocity $K_1(U_b)$ by introducing the ratio U_b/U_0, is obtained for all assessed L_t/d for $U_b > 3$ m/s. Accounting for the ratio U_b/U_0 allows to compensate in a crude way for different initial conditions at the nozzle exit.
- Furthermore, expressing the asymptotic mean centreline velocity decay coefficient as function of the bulk velocity $K_1(U_b)$ allows to approximate the decay as a function of initial turbulence intensity u_0/U_0 by a linear relationship which holds for $U_b > 3$ m/s regardless the length-to-diameter ratio L_t/d. The existence of a linear relationship for different nozzle geometries needs further validation.
- Decreasing the extension tube shortens the potential jet core extent due to the increased instability of the jet. In addition, an 'ad-hoc' criterion is proposed to determine the potential core extension x_{pc} as the maximum local Reynolds number along the centreline using a constant total jet spreading angle at the tube outlet of $\theta = 4.5°$.
- The previous observations are combined to provide a simple model with neglectable computational cost of the mean centreline velocity for known initial mean centreline velocity U_0 and length-to-diameter ratio L_t/d. Despite some crude approximations the model outcome has an error smaller than 10 % for all assessed geometrical and flow conditions.

References

1. Abdel-Rahman A, Al-Fahed S, Chakroun W (1996) The near-field characteristics of circular jets at low Reynolds numbers. Mech Res Commun 23:313–324
2. Ashforth-Frost S, Jambunathan K (1996) Effect of nozzle geometry and semi-confinement on the potential core of a turbulent axisymmetric free jet. Int Commun Heat Mass Transf 23:155–162
3. Batchelor GK (2000) An introduction to fluid dynamics. Cambridge mathematical library
4. Bodony D (2005) The prediction and understanding of jet noise. Center for Turbulence Research Annual Research Briefs, pp 367–377
5. Boguslawski L, Popiel CO (1979) Flow structure of the free round turbulent jet in the initial region. J Fluid Mech 90:531–539
6. Burattini P, Antonia R, Rajagopalan S, Stephens M (2004) Effect of initial conditions on the near-field development of a round jet. Exp Fluids 37:56–64
7. Crow SC, Champagne FH (1971) Orderly structure in jet turbulence. J Fluid Mech 48:547–591
8. Daniloff R, Schuckers G, Feth L (1980) The physiology of speech and hearing. Prentice Hall, New York
9. Drubka R, Reisenthel P, Nagib H (1989) The dynamics of low initial disturbance turbulent jets. Phys Fluids A 1:1723–1735
10. Fellouah H, Ball CG, Pollard A (2009) Reynolds number effects within the development region of a turbulent round free jet. Int J Heat Mass Transf 52:3943–3954
11. George WK (1989) The self-preservation of turbulent flows and its relation to initial conditions and coherent structures. In: Recent advances in turbulence. Hemisphere, New York, pp 39–73
12. George WK (1992) The decay of homogeneous isotropic turbulence. Phys Fluids A 4:1492–1509
13. Grandchamp X (2009) Modélisation physique des écoulements turbulents appliquée aux voies aériennes supérieures chez l'humain. PhD thesis. Grenoble University
14. Grandchamp X, Van Hirtum A, Pelorson X (2010) Hot film/wire calibration for low to moderate flow velocities. Meas Sci Technol 21:115402
15. Hill BJ (1972) Measurement of local entrainment rate in the initial region of axisymmetric turbulent air jets. J Fluid Mech 51:773–779
16. Howe M, McGowan R (2005) Aeroacoustics of [s]. Proc R Soc A 461:1005–1028
17. Hussein H, Capp S, George W (1994) Velocity measurements in a high Reynolds number momentum conserving axisymmetric turbulent jet. J Fluid Mech 258:31–75
18. Kwon SJ, Seo IW (2005) Reynolds number effects on the behavior of a non-buoyant round jet. Exp Fluids 38:801–812
19. Malmström TG, Kirkpatrick AT, Christensen B, Knappmiller KD (1997) Centreline velocity decay measurements in low-velocity axisymmetric jets. J Fluid Mech 246:363–377
20. Mi J, Kalt P, Nathan G, Wong C (2007) PIV measurements of a turbulent jet issuing from round sharp-edged plate. Exp Fluids 42:625–637

21. Mi J, Nathan G, Luxton R (2000) Centreline mixing characteristics of jets from nine differently shaped nozzles. Exp Fluids 28(2):93–94
22. Mi J, Nobes D, Nathan G (2001) Influence of jet exit conditions on the passive scalar field of an axisymmetric free jet. J Fluid Mech 432:91–125
23. Nottage HB (1951) Report on ventilation jets in room air distribution. Technical report. Case Inst. of Technology, Cleveland
24. Panchapakesan N, Lumley J (1993) Turbulence measurements in axisymmetric jets of air and helium. Part 1. Air jet. J Fluid Mech 246:197–224
25. Pitts W (1991) Reynolds number effects on the mixing behavior of axisymmetric turbulent jets. Exp Fluids 11:1432–1114
26. Quinn W (2006) Upstream nozzle shaping effects on near field flow in round turbulent free jets. Eur J Mech B, Fluids 25:279–301
27. Romano G, Antonia R (2001) Longitudinal and transverse structure functions in a turbulent round jet: effect of initial conditions and Reynolds number. J Fluid Mech 436:231–248
28. Russ S, Strykowski P (1993) Turbulent structure and entrainment in heated jets: the effect of initial conditions. Phys Fluids 5:3216–3225
29. Sautet J, Stepowski D (1995) Dynamic behavior of variable-density, turbulent jets in their near development fields. Phys Fluids 7(2):2796–2806
30. Schlichting H, Gersten K (2000) Boundary layer theory. Springer, Berlin
31. Stevens K (1998) Acoustic phonetics. MIT Press, London
32. Van Hirtum A, Grandchamp X, Pelorson X (2009) Moderate Reynolds number axisymmetric jet development downstream an extended conical diffuser: influence of extension length. Eur J Mech B, Fluids 28:753–760
33. Wygnanski I, Fiedler HE (1969) Some measurements in the self preserving jet. J Fluid Mech 38:577–612
34. Xu G, Antonia R (2002) Effect of different initial conditions on a turbulent round free jet. Exp Fluids 33:677–683